Modular Biodegradable Biomaterials from Surfactant and Polyelectrolyte Mixtures

Yakov Lapitsky,[†] Tasneem Zahir,[†] and Molly S. Shoichet*[,†,‡,§]

Department of Chemical Engineering & Applied Chemistry, University of Toronto, 200 College Street, Toronto, ON M5S 3E5, Canada, Department of Chemistry, University of Toronto, 80 St. George Street, Toronto, ON M5S 3H6, Canada, Institute of Biomaterials and Biomedical Engineering, University of Toronto, 164 College Street, Toronto, ON M5S 3G9, Canada

Received August 23, 2007; Revised Manuscript Received October 18, 2007

Polymeric assemblies are used in many biomaterials applications, ranging from drug-bearing nanoparticles to macroscopic scaffolds. Control over their biodegradation rates is usually achieved through synthetic modification of their molecular structure. As a simpler alternative, we exploit the associative phase separation in mixtures of bioderived surfactants and polyelectrolytes. The gel fiber scaffolds are formed via phase inversion, using a homologous series of fatty acid salts—sodium caprate (NaC_{10}), laurate (NaC_{12}), and myristate (NaC_{14}), and a water-soluble chitosan derivative, *N*-[(2-hydroxy-3-trimethylammonium)propyl] chitosan chloride (HTCC). Their dissolution times are modulated through the selection of the fatty acid molecule and vary in a predictable manner from minutes (for NaC_{10}—HTCC), to hours (for NaC_{12}—HTCC), to days (for NaC_{14}—HTCC). These variations are linked to differences in surfactant—polyelectrolyte binding strength and scale with the equilibrium binding constants of their mixtures. These fibers were found to be both cytocompatible and cell-adhesive using neural stem/progenitor cells, suggesting their potential for utility in biomedical applications.

1. Introduction

Biocompatible polymers are widely used in drug delivery and tissue engineering, where they form a variety of structures, through either chemical cross-linking or physical association, that range from nanoparticles to macroscopic scaffolds.[1–4] In many applications, it is important to control their degradation rates, which is usually achieved by incorporating hydrolytically or enzymatically cleavable groups into the polymer structure.[5–12] Biodegradable polymer constructs can also be prepared via reversible physical cross-linking, where the degradation rates depend on the strength of electrostatic, hydrophobic, or hydrogen bonding interactions.[13–16] Both of these approaches to tuning the degradation rates, however, have the disadvantage of usually requiring the polymer to be synthetically modified. An alternative approach is to control the degradation rates by using a modular physical cross-linker, the association strength of which will govern the degradation rate of the gel. This can be achieved by exploiting the association between biologically derived surfactants and polyelectrolytes.

Mixtures of oppositely charged surfactants and polyelectrolytes are commonplace in many commercial products. When mixed in aqueous environments, they self-assemble into a variety of soluble or insoluble structures, which range from viscous fluids,[17,18] to nanoparticles,[19–21] to macroscopic fibers,[22] coatings,[20,23] and beads.[24,25] Over the past decade, their application has also been explored in drug and gene delivery.[26–29] Their molecular association is driven by electrostatic interactions[30,31] and occurs at surfactant concentrations well below the critical micelle concentration (CMC).[31,32] These attractive interactions can cause associative phase separation, where a viscous liquid, gel, or precipitate forms in equilibrium with a dilute supernatant.[18,33,34]

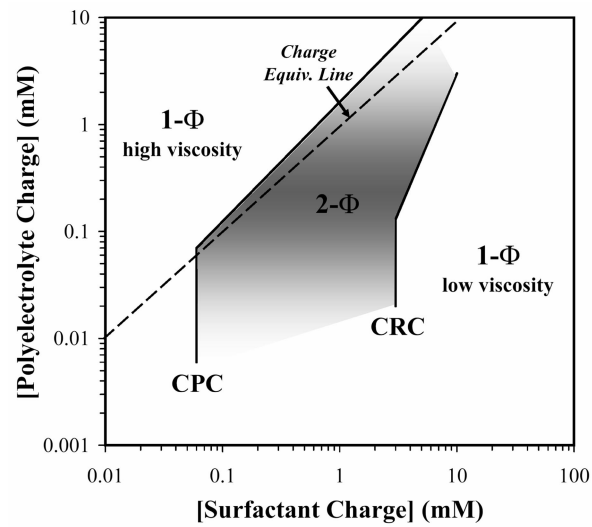

Figure 1. Phase map of the dilute cat-HEC—SDS—water mixtures (adapted from ref 35).

The equilibrium phase behavior of carbohydrate-based systems that form gel-like assemblies[22,24,25,35] is exemplified in Figure 1, which shows a phase map for dilute aqueous mixtures of the cationic, trimethylammonium derivatized hydroxyethyl cellulose (cat-HEC) and sodium dodecyl sulfate (SDS). When either the surfactant or the polyelectrolyte is in excess, the mixture forms a single-phase solution that is viscous when the mixture is polyelectrolyte-rich and nonviscous when it is surfactant-rich (Figure 1). When the oppositely charged species are mixed in more stoichiometric proportions, however, they

* Corresponding author. E-mail address: molly@ecf.utoronto.ca. Telephone: 1-416-978-1460. Fax: 1-416-978-4317. Address: 514 Donnelly Centre for Cellular and Biomolecular Research, 160 College Street, Toronto, Ontario M5S 3E1, Canada.

[†] Department of Chemical Engineering & Applied Chemistry, University of Toronto.

[‡] Department of Chemistry, University of Toronto.

[§] Institute of Biomaterials and Biomedical Engineering, University of Toronto.

10.1021/bm7009416 CCC: $40.75
Published on Web 12/19/2007

Scheme 1. Molecular Structure of *N*-[(2-Hydroxy-3-trimethylammonium) propyl] Chitosan Chloride (HTCC) Prepared from Partially Deacetylated Chitosan

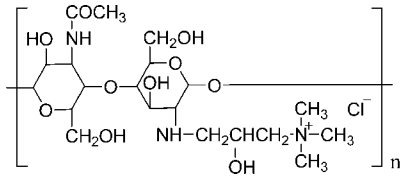

undergo associative phase separation and form a solid,[18,35] which can be used to form insoluble gel-like assemblies.[22,25,35] The phase behavior shown in Figure 1 yields two critical surfactant concentrations that are of practical importance: the critical precipitation concentration (CPC) and the critical redissolution concentration (CRC).[18,25,36] The CPC, which is given by the precipitation phase boundary in the limit of very low polyelectrolyte concentration,[18,36] marks the minimum surfactant concentration where associative phase separation begins to occur and is a measure of the surfactant−polyelectrolyte binding strength.[18,36] Likewise, the redissolution phase boundary in the limit of very low polyelectrolyte concentration indicates the CRC, that is, the surfactant concentration above which the gel phase ceases to be stable when immersed in an excess of supernatant solution.[25]

The strength of surfactant−polyelectrolyte binding and its colloidal and macroscopic consequences depend strongly on the hydrophobicity of the surfactant species.[32,34,37] Specifically, the surfactant−polyelectrolyte binding strength increases with the length of the surfactant tail.[18,32] This stronger binding shifts the CPC and the precipitation phase boundary to lower surfactant concentrations.[18,34,36] Likewise, an increase in surfactant tail length shifts the redissolution phase boundary in Figure 1 to significantly lower surfactant concentrations.[36] This tunability makes biocompatible surfactant−polyelectrolyte mixtures attractive as building blocks for modular drug delivery or tissue engineering scaffolds with highly tunable controlled degradation rates. However, their performance in this application remains largely unexplored.

Here, we demonstrate the preparation of cytocompatible surfactant−polyelectrolyte gel fibers (ranging between ca. 500 and 3000 μm in diameter), the degradation rates of which can be tuned over several orders of magnitude without synthetic modification. These versatile fibers show potential as either drug carriers or tissue engineering scaffolds and are formed via phase inversion of a viscous, polymer-rich surfactant−polyelectrolyte solution that is extruded into a low-viscosity surfactant solution.[22] Specifically, a water-soluble chitosan derivative, *N*-[(2-hydroxy-3-trimethylammonium) propyl] chitosan chloride (HTCC, see Scheme 1) is extruded into a homologous series of readily available, biologically derived fatty acid salts, sodium caprate (NaC_{10}), sodium laurate (NaC_{12}), or sodium myristate (NaC_{14}). HTCC is used because of its demonstrated potential as a drug carrier[38–40] and implant material that is both cytocompatible with mammalian cells and exhibits antibacterial properties.[41] The mechanism of gel degradation is dissolution, the times of which are modulated through the selection of the fatty acid molecule, range from minutes (for NaC_{10}−HTCC), to hours (for NaC_{12}−HTCC), to days (for NaC_{14}−HTCC), and are related to the differences in surfactant−polyelectrolyte binding strengths. Cytocompatibility and cell interaction with these fibers is demonstrated using rat brain derived neural stem cells.

2. Materials and Methods

2.1. Materials. All experiments were performed using Millipore Milli-Q deionized water with 18.2 MΩ cm resistivity. Highly viscous chitosan (MW = 500 000–700 000 g/mol) and glycidyltrimethylammonium chloride were purchased from Fluka (Buchs, Switzerland). Sodium caprate (NaC_{10}), sodium laurate (NaC_{12}), and sodium myristate (NaC_{14}) with respective minimum purities of 98%, 99%, and 99%, were purchased from Sigma-Aldrich (Oakville, ON, Canada). All materials were used as received.

2.2. HTCC Synthesis. *N*-[(2-Hydroxy-3-trimethylammonium)propyl]chitosan chloride (HTCC) was synthesized from chitosan using the protocol of Lim and Hudson.[42] Briefly, chitosan flakes (5 g) were dispersed in 195 mL of water at 85 ± 10 °C. Glycidyltrimethylammonium chloride (18.4 mL) was added under continuous stirring in three equal volumes at 2 h intervals, after which the dispersion was left to stir overnight. This resulted in a mixture of insoluble solvent-swollen flakes dispersed in a viscous polymer solution. The flakes were then removed via centrifugation. Using a Spectra/Por regenerated cellulose membrane (molecular weight cutoff = 3500), the soluble product was dialyzed for 24 h, twice against 10 mM NaCl, and three times against deionized water. To remove the residual solids, the dialyzed HTCC solution was filtered through a frit. The final product was then lyophilized and confirmed using ^{1}H NMR spectroscopy in deutarated water, where the reagent and product spectra (not shown) matched the literature spectra for chitosan and HTCC.[38]

2.3. HTCC Characterization. *2.3.1. Potentiometric Titration.* To quantify the polymer charge (and to determine the surfactant−polyelectrolyte stoichiometry used in the fiber preparation), potentiometric titrations of aqueous chitosan and HTCC solutions were done at room temperature using a Corning 320 pH meter equipped with an Acumet pH/ATC probe. Chitosan (37.6 mg) and HTCC (27.8 mg) were dissolved in 20.2 and 39.2 mL of water, respectively, whereupon neat HCl was added to achieve pH 2 (which is well below the pK_a values of chitosan and HTCC and results in fully protonated polymers). The solutions were then titrated with 20 mM NaOH solution up to pH 9, which was 3–5 units higher than the pK_a values of both polymers and results in full deprotonation of pH-sensitive charges.

2.3.2. Phase Behavior. Phase behavior of the fatty acid−HTCC mixtures was investigated at compositions relevant to gel fiber formation and dissolution. To determine the maximum surfactant loading in the viscous, polymer-rich fatty acid−HTCC mixtures used for fiber preparation, 0.8 wt % HTCC was mixed with various fatty acid compositions in water. To determine the critical redissolution concentration (above which the gel dissolves when immersed in excess supernatant), single drops (ca. 30 μL) of 1 wt % HTCC were added to 3 mL aqueous samples containing variable fatty acid compositions. Similarly, to determine the minimum surfactant concentrations necessary for the gel phase to be stable, CPCs were estimated for the fatty acid−HTCC mixtures at the physiological ionic strength and pH. To do this, the precipitation phase boundaries were measured in 1X phosphate buffered saline (PBS, pH 7.4) in the limit of very low HTCC concentration.[18] All mixtures were incubated for several days, either at room temperature (for polymer-rich mixtures and all mixtures containing NaC_{10}) or at 37 °C (for the less-soluble surfactant-rich mixtures containing NaC_{12} or NaC_{14}). The phase behavior was then recorded based on visual observations.

2.3.3. Rheology. Flow curves for 0.8 wt % HTCC dissolved in deionized water, or in aqueous solutions containing 0.8 wt % NaC_{10}, 0.4 wt % NaC_{12}, or 0.2 wt % NaC_{14} were obtained using an AR1000 stress controlled rheometer (TA Instruments, New Castle, DE) equipped with a 40 mm 2° cone. The samples were conditioned at 25 °C for 20 min prior to shear, whereupon their viscosities were measured at shear rates ranging from 0.05 to 800 s^{-1}. The zero-shear viscosities were then estimated by fitting the flow curves to the Carreau model using the instrument data analysis software.

2.4. Fiber Preparation. Approximately 0.5 mL of viscous fatty acid−HTCC mixtures (0.8 wt % HTCC mixed with either 0.8 wt %

Table 1. Solution Compositions Used for Fatty Acid−HTCC Fiber Preparation

fiber type	composition	extruded mixture	receiving solution	ion exchange solution
A	NaC_{10}−HTCC	0.8 wt % NaC_{10} 0.8 wt % HTCC	1.0 wt % NaC_{10}	N/A
B	NaC_{12}−HTCC	0.4 wt % NaC_{12} 0.8 wt % HTCC	0.5 wt % NaC_{12}	N/A
C	NaC_{14}−HTCC	0.2 wt % NaC_{14} 0.8 wt % HTCC	0.2 wt % NaC_{14}	N/A
D	NaC_{10}−HTCC	0.8 wt % NaC_{10} 0.8 wt % HTCC	0.5 wt % NaC_{10}	N/A
E	NaC_{12}−HTCC	0.8 wt % NaC_{10} 0.8 wt % HTCC	0.4 wt % NaC_{10} 0.1 wt % NaC_{12}	0.5 wt % NaC_{12}
F	NaC_{14}−HTCC	0.8 wt % NaC_{10} 0.8 wt % HTCC	0.4 wt % NaC_{10} 0.1 wt % NaC_{14}	0.15 wt % NaC_{14}

NaC_{10}, 0.4 wt % NaC_{12}, or 0.2 wt % NaC_{14}) were extruded through a 26 gauge syringe needle into Petri dishes (85 mm in diameter) filled with 30 mL of low-viscosity aqueous surfactant solutions, using the compositions in Table 1. As the surfactant diffused into the polymer-rich phase, the extruded jet gelled and fractured into 1–2 cm fibers. All NaC_{10}−HTCC fibers (fiber types A and D) were prepared by a single-step process (i.e., extruding the viscous NaC_{10}−HTCC mixture into a low-viscosity NaC_{10} solution) at room temperature and equilibrated for at least 2 h. NaC_{12}−HTCC and NaC_{14}−HTCC fibers were formed using either a one- or two-step method. In the single-step method used to form (fiber types B and C), the extruded jets of viscous NaC_{12}−HTCC or NaC_{14}−HTCC solutions were gelled in a solution of NaC_{12} or NaC_{14}, respectively, and left for at least 2 h to equilibrate. In the two-step method, fiber types E and F were first prepared by injecting viscous NaC_{10}−HTCC mixture into surfactant mixtures composed of 0.4 wt % NaC_{10} and 0.1 wt % of either NaC_{12} or NaC_{14} and left to equilibrate for 2 h. Then, to remove the weaker binding NaC_{10} from the HTCC, a second (ion exchange) step was carried out, where the fibers were immersed in 30 mL of either 0.5 wt % NaC_{12} or 0.15 wt % NaC_{14} for at least 2 h. Because the solubilities of NaC_{12} and NaC_{14} at room temperature are limited, their solutions were kept at 37 °C.

2.5. Fiber Degradation Visualization. To simulate gel degradation in model physiological environments, fiber dissolution was studied under both creeping flow and stagnant conditions. For degradation of fatty acid−HTCC fibers under creeping flow, fibers (0.5–1 cm in length and similar diameters, i.e., fiber types D−F) were inserted into clear tubes (4.54 mm ID). PBS was circulated through the tubes using a peristaltic pump at a rate of 6–7 mL/hr, which corresponds to a Reynolds number of approximately 0.3–0.4 ($Re = \rho Ud/\mu$, where ρ is the fluid density, U is the average fluid velocity, d is the inner diameter of the tube, and μ is the fluid viscosity). The fibers were observed at regular time intervals until they were no longer visible by eye. This time was recorded as the time of complete degradation. Likewise, the degradation times under stagnant conditions were measured by submersing the fibers in 30 mL of 1X PBS buffer and recording the time at which the fibers were no longer visible. Because surfactant−polyelectrolyte interactions exhibit a very weak temperature dependence,[34] the experiment was carried out at room temperature.

2.6. Assaying Cell−Fiber Interactions. *2.6.1. Isolation and Culture of Neural Stem Cells.* Neural stem/progenitor cells (NSCs) were isolated from the subependymal region of the lateral ventricles in the forebrain of adult enhanced green fluorescent protein (EGFP) transgenic male Wistar rats, as described previously.[43] Briefly, subependymal tissue was harvested from 8−12 week old rats and subjected to papain dissociation (Papain Dissociation System; Worthington Biochemical Corporation, Lakewood, NJ). The resulting cell suspension was resuspended in complete medium containing neurobasal media (Gibco-Invitrogen, Burlington, ON, Canada), B27 neural supplement (Gibco-Invitrogen), 2 mM L-glutamine (Sigma-Aldrich), 100 μg/mL penicillin−streptomycin (Sigma-Aldrich), 20 ng/ml epidermal growth factor (recombinant human EGF; Gibco-Invitrogen), 20 ng/ml basic fibroblast growth factor (recombinant human bFGF; Gibco-Invitrogen), and 2 ng/ml heparin (Sigma-Aldrich). Cell numbers and viability were determined with a hemocytometer and trypan blue exclusion test. Dissociated cells were plated in complete media and incubated at 37 °C in an incubator with 5% CO_2. GFP-positive neurospheres appeared in 2–3 weeks, after which cells were passaged every week.

2.6.2. Cell Adhesion. To study cell adhesion and spreading, 100 μL of neural stem cell suspension (1×10^5 cells/100 μL) was added to NaC_{12}−HTCC and NaC_{14}−HTCC fibers (fiber types E and F), which had been placed on sterile tissue culture treated glass coverslips in multiwell plates. The control wells contained 100 μL of neural stem cell suspension without fibers. The neural stem cells were cultured in complete medium either on fatty acid−HTCC fibers or alone for 24 h at 37 °C and 5% CO_2, after which they were counterstained with the nuclear dye 4′,6-diamidino-2-phenylindole (DAPI) present in Vectashield mounting media (Vector Laboratories, Burlingame, CA). The coverslips were then inverted and mounted onto glass slides. All samples were examined and photographed using an Olympus BX61 epifluorescent microscope. Each determination was performed in quadruplicate, and the experiment was repeated three times.

2.6.3. Cell Proliferation. Cell proliferation studies were carried out by plating neural stem cells at a density of 1×10^4 cells per well (or 3×10^3 cells/cm^2) in multiwell tissue culture plates. Three ca. 5 mm long NaC_{10}−HTCC, NaC_{12}−HTCC, or NaC_{14}−HTCC fibers (fiber types D−F) were added to 0.5 mL complete media contained in the Millicell hanging inserts (Biopore PTFE membrane, Millipore, Billerica, MA) present in each well. The resulting supernatant freely penetrated the insert membrane and was in direct contact with the neural stem cell suspension in the wells. The partitioning of the wells was carried out to allow luminescent quantification of cell proliferation, which would have been otherwise problematic due to the high optical density of the fibers. Cells were grown in the multiwell plates for 4 and 10 days, at the end of which the hanging well inserts were removed and cell growth was quantified using the CellTiter-Glo luminescent cell viability assay (Promega, Madison, WI). After 5 days, 0.5 mL of fresh media was added to the well inserts for the 10 days time point. This assay provides a homogeneous method of determining the number of viable cells in proliferation and cytotoxicity assays based on quantification of the ATP present, an indicator of metabolically active cells.

3. Results and Discussion

3.1. HTCC Characterization. *3.1.1. Aqueous HTCC.* Unlike chitosan, which is water-soluble only under acidic conditions (where its primary amine groups are protonated), HTCC dissolves in water at acidic, neutral, or basic pH due to the presence of positively charged quaternary amine groups (see Scheme 1). Although HTCC is nominally water-soluble,[38] as its concentration approaches 1 wt %, the solution becomes turbid. The turbidity indicates molecular aggregation and ultimately (over the course of days) results in a small amount

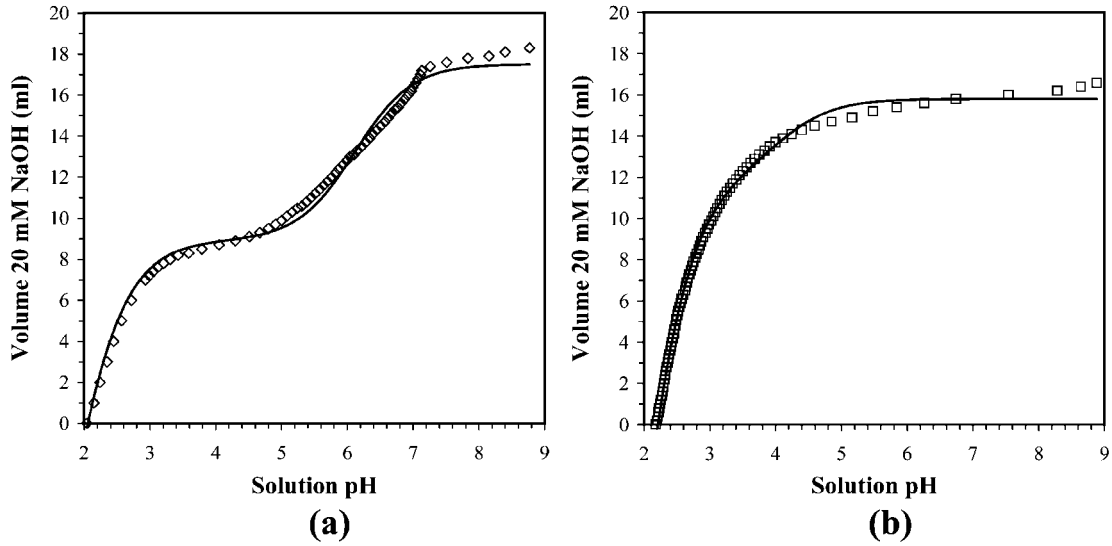

Figure 2. Potentiometric titration curves for (a) chitosan and (b) HTCC. The solid curves are the least-squares fits of eq 1, with R^2 values of (a) 0.9913 and (b) 0.9975.

of precipitate that is in equilibrium with a clear and viscous polymer-rich supernatant. This is consistent with previous studies, where the solution turbidity of HTCC formed from partially acetylated chitosan increased with decreasing charge density,[38] and likely can be prevented by fully deacetylating the chitosan prior to HTCC synthesis.[42]

To quantify the charge on HTCC and its parent chitosan, potentiometric titrations were performed on both the parent chitosan and HTCC product (see Figure 2a,b). Neglecting the dependence of polyelectrolyte pK_a values on the degree of protonation,[44,45] the number of charges, N_p (in moles), and their average pK_a values were estimated via least-squares-error fitting of the experimental data to the equation (see Appendix for derivation):

$$V^{add} = \frac{N_P\left(\frac{-10^{-pH}}{K_a + 10^{-pH}}\right) + N_{HCl}^{in} - V^{in}\left(10^{-pH} - \frac{K_w}{10^{-pH}}\right)}{C_{NaOH}^{Stock} + 10^{-pH} - \frac{K_w}{10^{-pH}}} \quad (1)$$

Here, C_{NaOH}^{Stock} is the concentration of the NaOH solution (20 mM), N_{Hcl}^{in} represents the amount of HCl initially added to lower the pH to ca. 2 (at which all titratable groups were protonated), K_w is the dissociation constant for water, V^{in} and V^{add} are the respective volumes of the initial chitosan/HCl solution and added NaOH, and 10^{-pH} expresses the H_3O^+ concentration in moles per liter. The fitted pK_a values for the chitosan and HTCC are 6.1 and 4.1, respectively. The lower pK_a of HTCC reflects the presence of its secondary amine (see Scheme 1), which replaces the primary amine of the parent chitosan and gives HTCC its pH sensitivity under acidic conditions.[40] Furthermore, Figure 2 shows that the buffering range of the polymer solution shifts from pH values of approximately 5–7, for chitosan, to approximately 3–5 for HTCC. This monotonic shift in the buffering range suggests the extent of primary amine conversion into secondary amines (i.e., conversion of chitosan into HTCC) to be high, consistent with the complete conversion reported by Lim and Hudson.[42] The N_P fits estimate that the native chitosan and HTCC bear 4.5×10^{-3} and 2.7×10^{-3} moles of charged monomer units per gram of polymer, respectively. Using this result, the degree of deacetylation (DD) of the parent chitosan was estimated to be 78% (in agreement with the 77% estimated by ^{1}H NMR and the 75–85% range reported by the manufacturer) using:

$$\frac{N_P}{m_P} = \frac{DD}{MW_A(1 - DD) + MW_D DD} \quad (2)$$

where, m_P is the mass of the titrated polymer, and MW_A (203 g/mol) and MW_D (160 g/mol) are the molecular weights of the acetylated and deacetylated repeat units, respectively. Similarly, assuming that the quaternization reaction achieved full conversion, the percentage of HTCC monomers bearing charge was estimated to be 73% using eq 2 and a MW_D of 311.5 g/mol (which is the molecular weight of the HTCC monomer unit). This estimate is within 10% of the result obtained for the parent chitosan, which is likely within the error margin of this first-order estimate and provides further evidence that the chitosan derivatization reaction is near complete conversion.

3.1.2. HTCC−Fatty Acid Interactions. Fatty acid−HTCC phase behavior was probed at timescales and compositions relevant for fiber formation and dissolution. Aqueous interactions between HTCC and fatty acid salts are qualitatively similar to those of the structurally similar cat-HEC with anionic surfactants,[17,18,25,46] which have been used for gel preparation in previous studies.[22,25,35] When dilute fatty acid−HTCC mixtures are rich in either surfactant or polyelectrolyte, they remain largely soluble (although small amounts of HTCC still precipitate). Conversely, at near-stoichiometric ratios, they undergo associative phase separation and yield a gel-like precipitate in equilibrium with a dilute supernatant. In polymer-rich fatty acid−HTCC mixtures that were used for fiber formation, the addition of surfactant increased the turbidity and amplified the viscosity of the 0.8 wt % HTCC (the zero-shear viscosity of which is 5 cP at 25 °C) by up to 1–2 orders of magnitude. The optical density and viscosity of the surfactant-rich mixtures, on the other hand, remain low.

Both the precipitation and redissolution phase boundaries shift to lower surfactant concentrations with increasing hydrophobicity (and association strength, see Table 2) of the fatty acid molecules. For weakly binding NaC_{10}−HTCC mixtures, macroscopic phase separation of 0.8 wt % HTCC solutions occur above ca. 0.8 wt % (41 mM) NaC_{10}, roughly twice the concentration of charged HTCC monomers (ca. 19 mM). The

Table 2. Fatty Acid Concentrations at Phase Boundaries Relevant to Gel Fiber Preparation

surfactant type	precipitation boundary in 0.8 wt % HTCC	CRC
NaC_{10}	0.8 wt % (41 mM)	>2 wt % (>100 mM)
NaC_{12}	0.4 wt % (18 mM)	0.6 wt % (27 mM)
NaC_{14}	0.3 wt % (12 mM)	0.2 wt % (8 mM)

stronger binding NaC_{12}−HTCC mixtures, however, phase separate at NaC_{12} concentrations above 0.4 wt % (18 mM NaC_{12}, i.e., near-equimolar proportions with the HTCC), and the strongest-binding NaC_{14}−HTCC mixtures precipitate at NaC_{14} concentrations above 0.3 wt % (12 mM). Likewise, the critical redissolution concentrations for the fatty acid−HTCC mixtures (i.e., the fatty acid concentrations that give rise to redissolution in the limit of very low polymer concentration[25]) are approximately 0.6 wt % and 0.2 wt % for NaC_{12} and NaC_{14}, respectively. Likewise, in agreement with the trend shown for the cat-HEC mixtures,[36] the critical redissolution concentration of dilute NaC_{10}−HTCC mixtures was higher than that of its homologues and was not observed in the NaC_{10} concentration range of interest (i.e., up to 2 wt %).

Additionally, because the gel fiber degradation rates depend on the fatty acid−HTCC binding strength under physiological conditions, the CPCs of the fatty acid−HTCC mixtures were approximated in PBS (pH 7.4). This was done by determining their precipitation phase boundaries in the limit of very low polyelectrolyte concentration, as has been previously described.[18] Figure 3 shows that the CPCs decrease exponentially with the fatty acid chain length, reflecting the stronger binding of the longer fatty acid molecules to the polyelectrolyte. The exponential trend is consistent with those reported for cat-HEC and alkyl sulfate mixtures.[18,36] Interestingly, this scaling with alkyl chain length is roughly inversely proportional to that exhibited by the surfactant−polyelectrolyte binding constant, *Ku*, which varies exponentially with the number of carbon atoms, *n*, according to:[18,32,34,36]

$$Ku = \exp\left(\frac{-(\Delta G^{o} + n\Phi)}{k_{B}T}\right) \quad (3)$$

Here, the Gibbs free energy of surfactant binding is given by $\Delta G^{o} + n\Phi$, where ΔG^{o} is a constant and Φ (the values of which typically range between –1.1 and −1.4 $k_{B}T$) is the free energy of transfer per hydrophobic CH_2 group.[18,32,37] Accordingly, the exponential fit of the fatty acid−HTCC data in Figure 3 yields a Φ value of −1.36 $k_{B}T$, which corresponds to a 3.9-fold variation in *Ku* per carbon atom in the fatty acid tail.

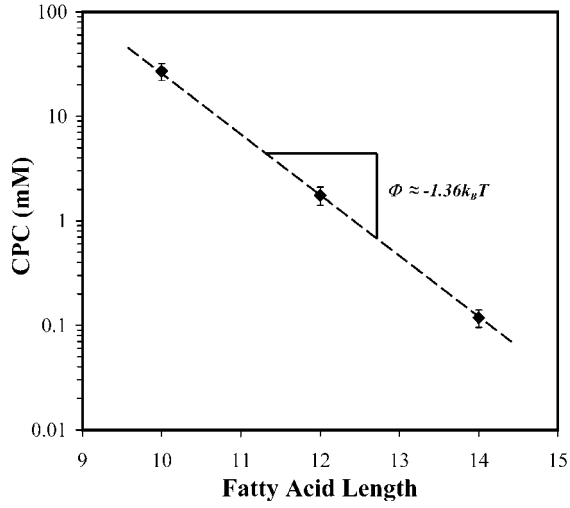

Figure 3. Fatty acid−HTCC CPCs in PBS plotted vs the fatty acid tail length. The error bars indicate the fatty acid concentrations of the samples directly above and below the phase boundary.

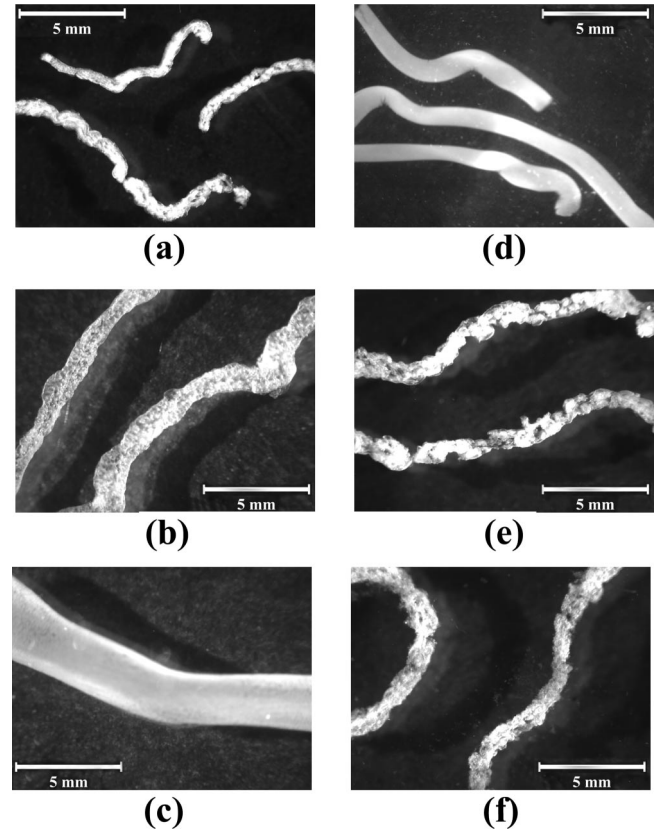

Figure 4. Dark-field micrographs of gel fibers (types A through F) prepared from HTCC and (a,d) NaC_{10}, (b,e) NaC_{12}, and (c,f) NaC_{14} using the (a−d) one-step and (e,f) two-step methods using the mixture compositions given in Table 1.

3.2. Fiber Formation. Surfactant−polyelectrolyte gel fibers were formed by extruding viscous, polymer-rich surfactant−polyelectrolyte mixtures into low-viscosity solutions of pure surfactant.[22] To minimize the deformation of the surfactant−polyelectrolyte solution jet prior to its gelation, the gelation process was accelerated by using solutions with higher surfactant concentrations. These concentrations, however, were limited by the phase boundaries described in Section 3.1.2. Consequently, the formation of stable fibers by a single-step process required the use of different surfactant concentrations for each surfactant species. Initially, fatty acid−HTCC fibers were prepared with the one-step method (fiber types A through C) using the solution compositions given in Table 1.

The fiber diameter and morphology (see Figure 4a,b,c) varied with the composition of the parent mixtures. The faster-gelling fibers that were formed using the more concentrated fatty acid solutions (e.g., NaC_{10}−HTCC, Figure 4a) had rougher morphologies, possibly reflecting a more rapid collapse of HTCC chains.[22] Conversely, the variations in fiber diameter (where thicker fibers formed from longer surfactants) were likely due to the osmotic swelling of the polyelectrolyte phase prior to gelation that occurs during phase inversion.[22] The osmotic pressures in the extruded fatty acid−HTCC mixtures with longer hydrocarbon tails were higher because fewer of the polyelectrolyte charges were neutralized by polymer-bound surfactant.[22] Likewise, the fatty acid concentrations and osmotic pressure in

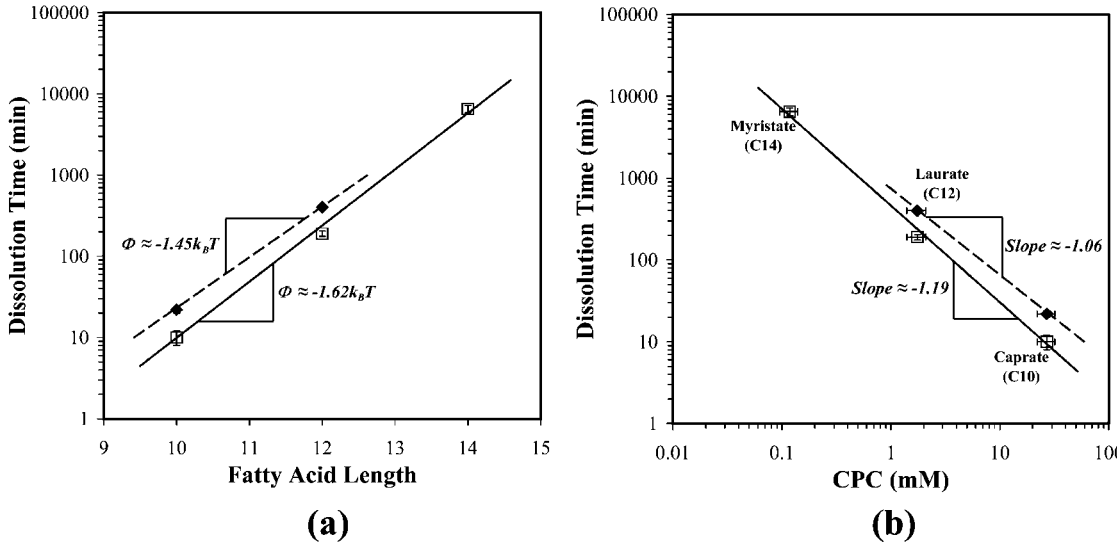

Figure 5. Fatty acid−HTCC fiber dissolution in (♦) stagnant and (□) flowing (Re = 0.3–0.4) 1X PBS buffer plotted vs (a) fatty acid tail length and (b) fatty acid CPCs. The error bars indicate the observation times immediately before and after fiber disintegration.

the receiving solutions were lower for the longer fatty acid molecules due to their lower critical redissolution concentrations. Moreover, the lower surfactant concentrations in the receiving solutions reduced the gelation rate and gave the fibers more time to swell. The combination of these factors amplified the extent of osmotic swelling and resulted in fiber diameters ranging from hundreds of micrometers (for NaC_{10}−HTCC fibers, Figure 4a) to millimeters (for NaC_{14}−HTCC fibers, Figure 4c).

Although these osmotic effects complicate the formation of homologous fibers with the same diameter, they can be overcome using a two-step process. Here, fibers are initially prepared using near-isoosmotic fatty acid−HTCC mixtures and then undergo a surfactant ion exchange step, which does not disturb the macroscopic structure of the fibers. Specifically, the fibers are first prepared using mostly NaC_{10} (the weakest-binding surfactant) by extruding 0.8 wt % HTCC with 0.8 wt % NaC_{10} into either 0.5 wt % NaC_{10} (for the production of NaC_{10}−HTCC fibers) or into a mixture of 0.4 wt % NaC_{10} with 0.1 wt % of either NaC_{12} or NaC_{14}, (for NaC_{12}−HTCC and NaC_{14}−HTCC fibers, respectively). Then, to replace the HTCC-bound NaC_{10} with NaC_{12} or NaC_{14}, the fibers were immersed in either 0.5 wt % NaC_{12} or 0.15 wt % NaC_{14}.

Parts d, e, and f of Figure 4 show that the diameters of the NaC_{10}−HTCC, NaC_{12}−HTCC, and NaC_{14}−HTCC fibers formed using the two-step process are all ca. 1 mm and are practically independent of the fatty acid type. However, fibers produced using NaC_{10}/NaC_{12} or NaC_{10}/NaC_{14} mixtures have significantly rougher morphologies than their NaC_{10}−HTCC homologue. This may result from the more rapid gel collapse that is predicted for stronger-binding surfactants, such as NaC_{12} or NaC_{14}.[22]

3.3. Fiber Degradation Rates. To investigate the stability of fatty acid−HTCC gels under model physiological conditions, fiber dissolution times were tracked in PBS buffer both under stagnant and creeping flow conditions (Re = 0.3–0.4). Dissolution times under creeping flow varied exponentially with the length of the fatty acid tail (see Figure 5a) from minutes for NaC_{10}−HTCC fibers, to hours for NaC_{10}−HTCC fibers, to days for NaC_{14}−HTCC fibers. The dissolution times for NaC_{10}−HTCC and NaC_{12}−HTCC fibers in stagnant PBS appeared to follow similar scaling and were approximately twice as long as that under flow. The NaC_{14}−HTCC fibers, however, never completely dissolved. These results reflect the differences in the surfactant−polyelectrolyte binding strength and can be interpreted using a simple mass transfer analysis. Because the HTCC only becomes soluble upon surfactant desorption, the dissolution rate is inversely proportional to the rate of surfactant elution. As a first-order approximation, the elution rate, N_A, can be quantified by the expression:[47]

$$N_A = k_m a(C_A^{fiber} - C_A^{bulk}) \quad (4)$$

where k_m is the mass transfer coefficient (which depends on the surfactant diffusivity and the hydrodynamic environment of the PBS solution), a is the interfacial area through which the surfactant is eluted, and C_A^{fiber} and C_A^{bulk} are the free surfactant concentrations in the fiber and the bulk supernatant, respectively. C_A^{fiber} depends on the binding strength of the surfactant−polyelectrolyte system and, although surfactant−polyelectrolyte binding is cooperative,[32,48,49] for simplicity it can be related to the fractional coverage of the polyelectrolyte binding sites with the Langmuir isotherm:

$$C_A^{fiber} = \frac{\beta}{Ku(1 - \beta)} \quad (5)$$

where Ku is the binding constant and β represents the fractional coverage of the polyelectrolyte sites. Given that for an excess of supernatant solution, C_A^{bulk} is much smaller than C_A^{fiber}, the elution rate equation can be rewritten as

$$N_A = k_m a \frac{\beta}{Ku(1 - \beta)} \quad (6)$$

Thus, the rate of surfactant elution is inversely proportional to Ku, which varies exponentially with the number of carbon atoms according to eq 3. Consequently, it follows that $N_A \propto k_m e^{n\Phi}$ and the dissolution time in Figure 5a scales exponentially with the number of carbon atoms in the fatty acid molecule. Moreover, assuming that the mass transfer coefficient varies little with surfactant length, Φ values can be fitted to this experimental data for both stagnant and flowing environments as −1.45 and −1.62 k_BT, respectively. These are lower than those fitted from the CPC values in Section 3.1.2 and correspond to a 4- to 5-fold increase in dissolution time per surfactant CH_2 group.

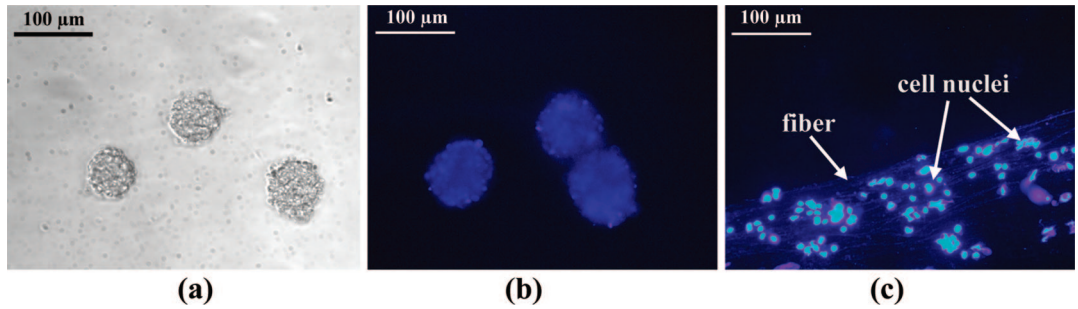

Figure 6. NSCs grown as neurospheres imaged via (a) bright field and (b) fluorescence microscopy (after DAPI staining) and (c) DAPI-stained NSCs adhered to a NaC_{14}−HTCC fiber.

The inverse relationship between the CPC and the binding constant, *Ku*, suggests that the dissolution times can be predicted from the CPC of the surfactant−polyelectrolyte mixture. Figure 5b shows that the experimental scaling exponents between the dissolution time and CPC for dissolution under stagnant conditions and under creeping flow are −1.06 and −1.19, respectively, and are in reasonable agreement with the expected inverse proportionality. The minor discrepancies in these scaling exponents and Φ values (which are amplified in the presence of flow) might reflect the slight differences in k_m between the fibers, caused by the differences in fiber roughness and fatty acid structure. Similarly, the roughly 2-fold rise in dissolution time between flowing and stagnant conditions is caused by the amplification in k_m with increasing supernatant flow rate.

The NaC_{14}−HTCC fibers never completely dissolved under stagnant conditions because the equilibrium NaC_{14} concentration inside the 30 mL PBS vial was above the precipitation phase boundary for the strongly binding NaC_{14}−HTCC system. This illustrates the effect of confinement on the degradation of physically associated scaffolds. When the fiber is contacted with a limited supernatant volume, C_A^{bulk} may rise to a value that is no longer negligible, and when C_A^{bulk} is equal to C_A^{fiber}, fiber dissolution stops. Thus, using the surfactant−polyelectrolyte Langmuir binding isotherm, the minimum volume necessary to completely dissolve the fibers, V_{min}, can be roughly estimated as a function of *Ku* and the β value necessary for phase separation ($\beta_{2\varphi}$) to occur as:

$$V_{min} = \frac{KuN_S^{in}(1 - \beta_{2\varphi})}{\beta_{2\varphi}} \quad (7)$$

where N_S^{in} represents the number of moles of surfactant initially present in the fiber. Hence, (if $\beta_{2\varphi}$ is constant) the minimum volume needed to completely dissolve NaC_{14}−HTCC fibers is roughly 15 times higher than that of NaC_{12}−HTCC and 230 times higher than that of NaC_{10}−HTCC.

3.4. Cell−Fiber Interactions. When rat brain-derived neural stem/progenitor cells (NSCs) were seeded as neurospheres on NaC_{12}−HTCC and NaC_{14}−HTCC fibers for 24 h, they adhered to the fibers and a large percentage of the neurosphere-forming cells migrated out from their original aggregates onto the fiber surfaces. This migration demonstrates a common feature of neurospheres when the cells interact favorably with the substrate.[50] Parts a and b of Figure 6 show bright field and DAPI-stained fluorescent micrographs of NSCs growing as free floating spheres prior to being seeded onto the fibers. Their attachment and spreading on NaC_{14}−HTCC fibers is illustrated in Figure 6c, which depicts DAPI-stained cell nuclei dispersed on the surface of a weakly fluorescent fiber 24 h after plating. Similar results were observed on the NaC_{12}−HTCC. The

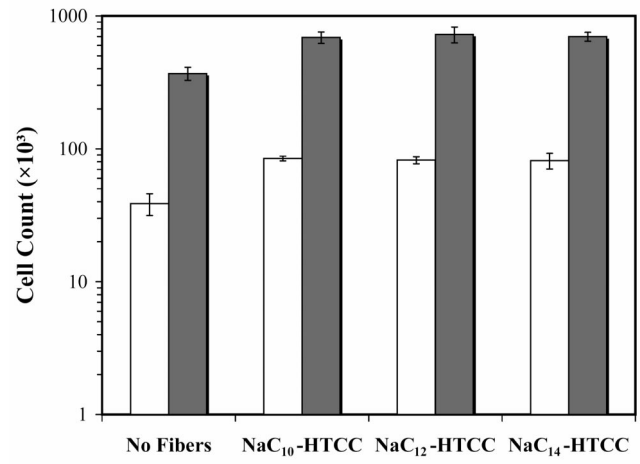

Figure 7. NSC counts with and without the fatty acid−HTCC fibers (□) 4 and (■) 10 days after plating.

NaC_{10}−HTCC fibers were not assayed for direct cell adhesion and spreading because they degraded too quickly.

Fiber cytotoxicity was tested by quantifying NSC proliferation in the absence and presence of fatty acid−HTCC fibers 4 and 10 days after plating. Because the fibers have a high optical density, the assay was carried out using sectioned wells where the cells were separated from the fibers by a porous PTFE membrane that was permeable to the fiber supernatant. This enabled luminescent quantification of the effects of fatty acids and HTCC on cell growth. When the fibers were introduced, the NaC_{10}−HTCC fibers underwent rapid dissolution, whereas NaC_{12}−HTCC and NaC_{14}−HTCC fibers remained mostly intact for several days. The neurospheres growing in the fiber-free control wells fused over time into very large aggregates, ranging approximately 300–500 μm in diameter. In contrast, the sample wells with the fibers contained smaller, uniform 50–100 μm spheres, which grew in size and number but did not fuse together as the cell density increased over time. This was likely caused by the elution of fatty acids from the gel fibers. Interestingly, the neurospheres grown in the presence of fast-degrading NaC_{10}−HTCC fibers adhered to the bottom of the wells. This may be due to the adsorption of cell-adhesive HTCC onto the well surface after the NaC_{10}−HTCC fibers dissolve.

Figure 7 indicates that all samples containing fibers exhibited cell counts double that of the fiber-free control, and a roughly 10-fold population growth between the 4- and 10-day time points. The lower levels of proliferation in the fiber-free control may have been due to the limited diffusion of nutrients into the inner cores of the very large aggregates that formed.[51] Thus, the cell counts suggest that all three surfactant−polyelectrolyte systems were cytocompatible with the NSCs. The cytocompatibility of the HTCC is consistent with the literature data obtained

using 3T3 mouse fibroblast,[41] and provides further evidence of the polymer's usefulness as a cytocompatible implant with antibacterial properties.[41] Likewise, the fatty acids were not detrimental to NSC proliferation, although they are known to be cytotoxic when present in high concentrations.[52] The lack of cytotoxicity observed for the fatty acids may be due to their association with HTCC, which lowers the concentration of free fatty acid molecules in contact with the cells.

4. Conclusions

The associative interactions between oppositely charged bioderived surfactants and polyelectrolytes such as fatty acids and the water-soluble chitosan derivative, HTCC, can be exploited to produce gel-like fibers with highly tunable degradation rates. These fibers are cytocompatible and cell adhesive with neural stem/progenitor cells. Fiber degradation occurs via dissolution and depends on the rate at which the surfactant elutes from the gel. Consequently, gel degradation times can be modulated in a predictable manner from minutes to days by varying the hydrophobicity of surfactants that belong to a homologous series. These times increase exponentially with the number of carbon atoms in its hydrophobic tail, linearly with the surfactant−polyelectrolyte binding constant and inversely with the critical precipitation concentration. This predictable tunability suggests that surfactant−polyelectrolyte gels offer an attractive and versatile alternative to traditional ways of creating biodegradable polymeric biomaterials, ranging from rapidly degrading drug carriers to longer-lasting tissue engineering scaffolds.

Appendix

The model equation used to fit the results in the potentiometic titration experiments (eq 1) was derived using mass action expressions (eqs A.1 and A.2), mass balances (eqs A.3 A.7), and the overall charge balance (eqs A.8 or A.9).

$$K_a = \frac{[H_3O^+][P]}{[P^+]} \quad (A.1)$$

$$K_w = [H_3O^+][OH^-] \quad (A.2)$$

$$C_P^{tot} = [P] + [P^+] \quad (A.3)$$

$$C_{HCl}^{tot} = [Cl^-]\ (\text{for chitosan}) \quad (A.4)$$

$$C_P^{tot} + C_{HCl}^{tot} = [Cl^-]\ (\text{for HTCC}) \quad (A.5)$$

$$C_P^{tot} = [QP^+]\ (\text{for HTCC}) \quad (A.6)$$

$$C_{NaOH}^{total} = [Na^+] \quad (A.7)$$

$$[P^+] + [H_3O^+] + [Na^+] = [OH^-] + [Cl^-](\text{for chitosan}) \quad (A.8)$$

$$[P^+] + [QP^+] = [H_3O] + [Na^+] = [OH^-] + [Cl^-](\text{for HTCC}) \quad (A.9)$$

Here, $[P^+]$, $[P]$, and $[QP^+]$ represent the concentrations of protonated amines, deprotonated amines, and quaternary amines, repectively. The differences between the material balance equations for the two titrations are due to the quaternary amine and chloride ions present on each charge-bearing HTCC monomer. Because this group does not affect the acid–base equilibrium however, it does not affect the ultimate analytical result. After a series of substitutions, a relationship between C_P^{tot}, C_{NaOH}^{tot}, C_{HCl}^{tot}, and the solution pH for both polymers is constructed:

$$C_P^{tot} = \frac{10^{-pH} + C_{NaOH}^{tot} - \frac{K_w}{10^{-pH}} - C_{HCl}^{tot}}{\frac{-10^{-pH}}{K_a + 10^{-pH}}} \quad (A.10)$$

To express this relationship in terms of the added volume of NaOH solution, C_P^{tot}, C_{NaOH}^{tot}, and C_{HCl}^{tot} are written in terms of moles and volumes as:

$$C_P^{tot} = \frac{N_P^{in}}{V^{in} + V^{add}} \quad (A.11)$$

$$C_{HCl}^{tot} = \frac{N_{HCl}^{in}}{V^{in} + V^{add}} \quad (A.12)$$

$$C_{NaOH}^{tot} = \frac{C_{NaOH}^{Stock} V^{add}}{V^{in} + V^{add}} \quad (A.13)$$

Substituting these equations into eq A.10 and solving for V^{add} yields the final result:

$$V^{add} = \frac{N_P\left(\frac{-10^{-pH}}{K_a + 10^{-pH}}\right) + N_{HCl}^{in} - V^{in}\left(10^{-pH} - \frac{K_w}{10^{-pH}}\right)}{C_{NaOH}^{Stock} + 10^{-pH} - \frac{K_w}{10^{-pH}}} \quad (A.14)$$

Acknowledgment. We gratefully acknowledge R. G. Wylie for NMR support, E. Kumacheva, and H. Zhang for providing an HTCC sample for the preliminary work, and E. W. Kaler for fruitful discussions. We are grateful to Natural Sciences and Engineering Research Council (NSERC), Canadian Institutes of Health Research (CIHR), Canadian Stroke Network (CSN), and Advanced Food and Materials Network (AFMNet) for partial funding.

References and Notes

(1) Drury, J. L.; Mooney, D. J. *Biomaterials* **2003**, *24*, 4337.
(2) Langer, R.; Peppas, N. A. *AIChE J.* **2003**, *49*, 2990.
(3) Muzzarelli, R. A. A.; Muzzarelli, C. *Adv. Polym. Sci.* **2005**, *186*, 151.
(4) Rinaudo, M. *Macromol. Symp.* **2006**, *245–246*, 549.
(5) Bryant, S. J.; Anseth, K. S. *J. Biomed. Mater. Res.* **2003**, *64A*, 70.
(6) Burdick, J. A.; Chung, C.; Jia, X.; Randolph, M. A.; Langer, R. *Biomacromolecules* **2005**, *6*, 386.
(7) Levesque, S. G.; Shoichet, M. S. *Bioconjugate Chem.* **2007**, *18*, 874.
(8) Metters, A.; Hubbell, J. *Biomacromolecules* **2005**, *6*, 290.
(9) Rydholm, A. E.; Reddy, S. K.; Anseth, K. S.; Bowman, C. N. *Biomacromolecules* **2006**, *7*, 2827.
(10) Skarja, G. A.; Woodhouse, K. A. *J. Biomater. Sci., Polym. Ed.* **2001**, *12*, 851.
(11) Timmer, M. D.; Ambrose, C. G.; Mikos, A. G. *Biomaterials* **2003**, *24*, 571.
(12) Yu, L. M. Y.; Kazazian, K.; Shoichet, M. S. *J. Biomed. Mater. Res.* **2007**, *82A*, 243.
(13) Gupta, D.; Tator, C. H.; Shoichet, M. S. *Biomaterials* **2006**, *27*, 2370.
(14) Kong, H. J.; Alsberg, E.; Kaigler, D.; Lee, K. Y.; Mooney, D. J. *Adv. Mater.* **2004**, *16*, 1917.
(15) Lynn, D. M. *Soft Matter* **2006**, *2*, 269.
(16) Tate, M. C.; Shear, D. A.; Hoffman, S. W.; Stein, D. G. *Biomaterials* **2001**, *22*, 1113.
(17) Chronakis, I. S.; Alexandridis, P. *Macromolecules* **2001**, *34*, 5005.
(18) Goddard, E. D. *Colloids Surf.* **1986**, *19*, 301.

(19) Nizri, G.; Magdassi, S.; Schmidt, J.; Cohen, Y.; Talmon, Y. *Langmuir* **2004**, *20*, 4380.
(20) Thunemann, A. F. *Prog. Polym. Sci.* **2002**, *27*, 1473.
(21) Trabelsi, S.; Guillot, S.; Raspaud, E.; Delsanti, M.; Langevin, D.; Boue, F. *Adv. Mater.* **2006**, *18*, 2403.
(22) Lapitsky, Y.; Kaler, E. W. *Colloids Surf., A* **2006**, *282–283*, 118.
(23) Cao, W.; Yang, L.; Luo, H. *J. Appl. Polym. Sci.* **1998**, *70*, 1817.
(24) Babak, V. G.; Merkovich, E. A.; Galbraikh, L. S.; Shtykova, E. V.; Rinaudo, M. *Mendeleev Commun.* **2000**, *3*, 94.
(25) Lapitsky, Y.; Kaler, E. W. *Colloids Surf. A* **2004**, *250*, 179.
(26) Mel'nikov, S. M.; Dias, R.; Mel'nikova, Y.; Marques, E. F.; Miguel, M. G.; Lindman, B. *FEBS Lett.* **1999**, *453*, 113.
(27) Mel'nikov, S. M.; Sergeyev, V. G.; Yoshikawa, K. *J. Am. Chem. Soc.* **1995**, *117*, 2401.
(28) Moran, M. C.; Miguel, M. G.; Lindman, B. *Langmuir* **2007**, *23*, 6478.
(29) Thunemann, A. F.; General, S. *J. Conrolled Release* **2001**, *75*, 237.
(30) Hansson, P. *Langmuir* **2001**, *17*, 4167.
(31) Konop, A. J.; Colby, R. H. *Langmuir* **1999**, *15*, 58.
(32) Malovikova, A.; Hayakawa, K.; Kwak, J. C. T. *J. Phys. Chem.* **1984**, *88*, 1930.
(33) Piculell, L.; Lindman, B. *Adv. Colloid Interface Sci.* **1992**, *41*, 149.
(34) Thalberg, K.; Lindman, B. *J. Phys. Chem.* **1989**, *93*, 1478.
(35) Lapitsky, Y.; Eskuchen, W. J.; Kaler, E. W. *Langmuir* **2006**, *22*, 6375.
(36) Goddard, E. D.; Hannan, R. B. *J. Am. Oil Chem. Soc.* **1977**, *54*, 561.
(37) Matulis, D.; Rouzina, I.; Bloomfield, V. A. *J. Am. Chem. Soc.* **2002**, *124*, 7331.
(38) Cho, J.; Grant, J.; Piquette-Miller, M.; Allen, C. *Biomacromolecules* **2006**, *7*, 2845.
(39) Xu, Y.; Du, Y.; Huang, R.; Gao, L. *Biomaterials* **2003**, *24*, 5015.
(40) Zhang, H.; Mardyani, S.; Chan, W. C. W.; Kumacheva, E. *Biomacromolecules* **2006**, *7*, 1568.
(41) Shi, Z.; Neoh, K. G.; Kang, E. T.; Wang, W. *Biomaterials* **2006**, *27*, 2440.
(42) Lim, S. H.; Hudson, S. M. *Carbohydr. Res.* **2004**, *339*, 313.
(43) Zahir, T.; Nomura, H.; Guo, X. D.; Kim, H.; Tator, C. H.; Morshead, C. M.; Shoichet, M. S. *Cell Transplantation*; 2007, in press.
(44) Cesaro, A.; Paoletti, S.; Benegas, J. C. *Biophys. Chem.* **1991**, *39*, 1.
(45) Petrov, A. I.; Antipov, A. A.; Sukhorukov, G. B. *Macromolecules* **2003**, *36*, 10079.
(46) Goddard, E. D.; Hannan, R. B. *J. Colloid Interface Sci.* **1976**, *55*, 73.
(47) Cussler, E. L. *Diffusion: Mass Transfer in Fluid Systems*; Cambridge University Press: New York, 1997.
(48) Hayakawa, K.; Kwak, J. C. T. *J. Phys. Chem.* **1982**, *86*, 3866.
(49) Satake, I.; Yang, J. T. *Biopolymers* **1976**, *15*, 2263.
(50) Kearns, S. M.; Laywell, E. D.; Kukekov, V. K.; Steindler, D. A. *Exp. Neurol.* **2003**, *182*, 240.
(51) Plotnikov, E. Y.; Marei, M. V.; Podgornyi, O. V.; Aleksandrova, M. A.; Zorov, D. B.; Sukhikh, G. T. *Bull. Exp. Biol. Med.* **2006**, *141*, 142.
(52) Lima, T. M.; Kanunfre, C. C.; Pompeia, C.; Verlengia, R.; Curi, R. *Toxicol. in Vitro* **2002**, *16*, 741.

BM7009416